

# Smart *PZT*-interface for wireless impedance-based prestress-loss monitoring in tendon-anchorage connection

Khac-Duy Nguyen and Jeong-Tae Kim\*

*Department of Ocean Engineering, Pukyong National University, Busan 608-737, Korea*

*(Received November 8, 2011, Revised May 11, 2012, Accepted May 17, 2012)*

**Abstract.** For the safety of prestressed structures such as cable-stayed bridges and prestressed concrete bridges, it is very important to ensure the prestress force of cable or tendon. The loss of prestress force could significantly reduce load carrying capacity of the structure and even result in structural collapse. The objective of this study is to present a smart *PZT*-interface for wireless impedance-based prestress-loss monitoring in tendon-anchorage connection. Firstly, a smart *PZT*-interface is newly designed for sensitively monitoring of electro-mechanical impedance changes in tendon-anchorage subsystem. To analyze the effect of prestress force, an analytical model of tendon-anchorage is described regarding to the relationship between prestress force and structural parameters of the anchorage contact region. Based on the analytical model, an impedance-based method for monitoring of prestress-loss is conducted using the impedance-sensitive *PZT*-interface. Secondly, wireless impedance sensor node working on Imote2 platforms, which is interacted with the smart *PZT*-interface, is outlined. Finally, experiment on a lab-scale tendon-anchorage of a prestressed concrete girder is conducted to evaluate the performance of the smart *PZT*-interface along with the wireless impedance sensor node on prestress-loss detection. Frequency shift and cross correlation deviation of impedance signature are utilized to estimate impedance variation due to prestress-loss.

**Keywords:** prestress-loss; tendon-anchorage; electro-mechanical impedance; smart *PZT*-interface; wireless impedance sensor; structural health monitoring

---

## 1. Introduction

Prestressed structures have been widely constructed in many places in the world. Dealing with prestressing techniques, structures can be bigger, larger and even slimmer. However, risks following with these techniques may lead to undesirable situations since the loss of prestress forces results in significant reduction of load carrying capacity and even collapse of the structure. The reasons causing prestress-loss include shrinkage and creep in concrete, relaxation of cable stress, corrosion of tendon and anchorage, and failure of anchorage components. Therefore, monitoring of prestress force becomes an important issue to study for the safety of the structure.

Over the past two decades, the demand of structural health monitoring (*SHM*) has been increased in aerospace and civil infrastructures (Sohn *et al.* 2003, Yun and Min 2010). Among a variety of *SHM* studies, many researchers have focused on monitoring of prestress force by using global and local dynamic characteristics (Zui *et al.* 1996, Kim and Park 2007, Kim *et al.* 2009, Li *et al.* 2009,

---

\*Corresponding author, Professor, E-mail: [idis@pknu.ac.kr](mailto:idis@pknu.ac.kr)

Kim *et al.* 2010, Park *et al.* 2010). The global method usually utilizes acceleration responses to monitor cable-anchorage force, but not very sensitive to small prestress-loss. On the other hand, impedance-based local *SHM* is found to be very promising to capture small incipient change of structural parameters. The impedance-based method was first proposed by Liang *et al.* (1994). Since then, many researchers have improved the method and applied the method to various damage detection problems such as pipeline system (Park *et al.* 2001), thin circular plate (Zagrai and Giurguitiu, 2001), concrete beam and frame (Bhalla *et al.* 2003, Yang *et al.* 2008), plate girder bridge (Kim *et al.* 2006), and bolted connection (Mascarenas 2006). The method utilizes electro-mechanical impedance of *PZT*-structure system in high frequency responses to monitor structural change at critical region. The change in electro-mechanical impedance due to structural damage is usually quantified by statistical index (Sun *et al.* 1995, Zagrai and Giurguitiu 2001, Fasel *et al.* 2005) or by impedance shift at resonance (Mascarenas 2006, Kim *et al.* 2010). For prestress-loss monitoring in tendon-anchorage connection, Kim *et al.* (2010) applied impedance-based method to detect pattern change in impedance of anchorage. The variation of prestress force was well identified with the variation of impedance. However, the concept of the mechanism was not clearly explained.

This study presents a smart *PZT*-interface for wireless impedance-based prestress-loss monitoring in tendon-anchorage connection. Firstly, a smart *PZT*-interface is newly designed for sensitively monitoring of electro-mechanical impedance changes in tendon-anchorage subsystem. To analyze the effect of prestress force, an analytical model of tendon-anchorage is described regarding to the relationship between prestress force and structural parameters of the anchorage contact region. Based on the analytical model, an impedance-based monitoring of prestress-loss is conducted using the impedance-sensitive *PZT*-interface. Secondly, wireless impedance sensor node working on Imote2 platform, which is interacted with the smart *PZT*-interface, is outlined. Finally, experiment on a lab-scale tendon-anchorage of a prestressed concrete girder is conducted to evaluate the performance of the smart *PZT*-interface along with the wireless impedance sensor node on prestress-loss detection. Frequency shift and cross correlation deviation of impedance signature are utilized to estimate impedance variation due to prestress-loss.

## 2. Smart *PZT*-interface for prestress-loss monitoring

### 2.1 Impedance-based monitoring of tendon-anchorage prestress-loss

#### 2.1.1 Analysis of prestress force in tendon-anchorage

A system of tendon-anchorage under prestress force can be modeled by connection components (i.e., bearing plate, anchor block, tendon) and contact forces in equilibrium condition, as shown in Fig. 1(a). Prestress force is modeled by tendon force acting on the anchor block, and transformed to contact pressure and bearing stress in the interface of anchor block and bearing plate. On the other hand, according to contact mechanism (Johnson 1985), the interaction in the contact interface of bearing plate and anchor block can be simplified by two-dimensional damping (i.e., normal and transverse damping coefficient  $c_n$ ,  $c_u$ ) and spring stiffness (i.e., normal and transverse spring constant  $k_n$ ,  $k_u$ ), as shown in Fig. 1(b). Basically, the interfacial spring stiffness and damping values represent the amount of contact pressure and stress field acting at the interface. In the previous study by Ritdumrongkul *et al.* (2004), as shown in Fig. 2, it was reported that the variation of interfacial stiffness and damping parameters are associated with the variation of contact pressure

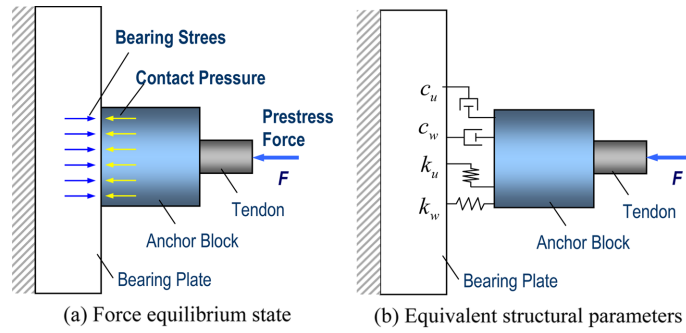
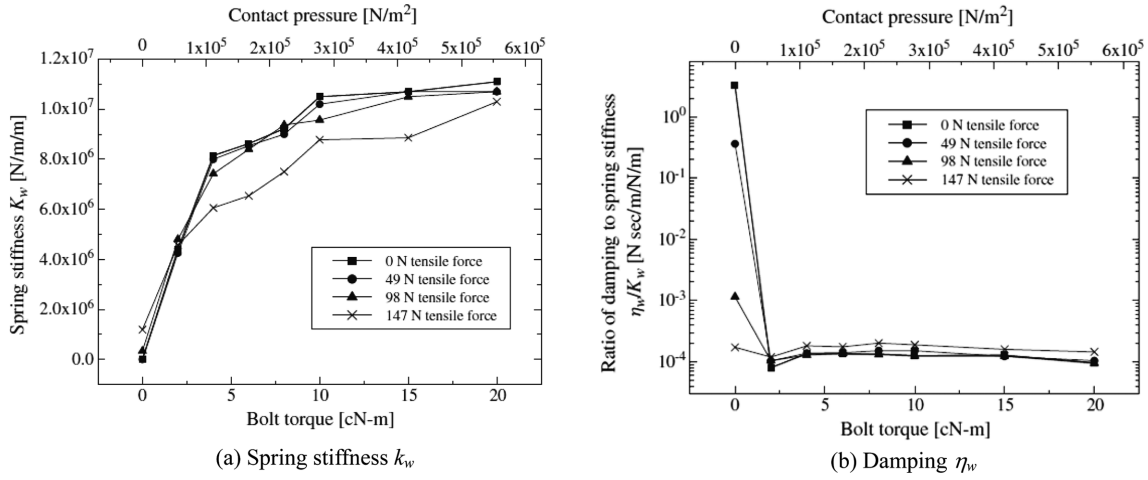


Fig. 1 Analytical model of tendon-anchorage at contact interface


 Fig. 2 Contact pressure versus structural parameters (Ritdumrongkul *et al.* 2004)

which is generated from bolt torque. For example, in their case, the contact pressure  $3 \times 10^5 \text{ N/m}^2$  was equivalent to  $1.0 \times 10^7 \text{ N/m}$  of normal spring stiffness  $k_w$  (Fig. 2(a)), and to  $1.0 \times 10^3 \text{ N.sec/m}$  of normal damping  $\eta_w$  (or  $c_w$ ) (Fig. 2(b)). Therefore, the variation of prestress force can be treated as the variation of those structural parameters at the contact interface.

### 2.1.2 Impedance-based monitoring method

To monitor structural change, a piezoelectric material (e.g., *PZT*) is surface-bonded to structure at examined region. The interaction between the *PZT* and the structure is simply explained by 1-D free-body diagram of *PZT*-structure system as shown in Fig. 3. Due to inverse piezoelectric effect, an input harmonic voltage  $V(\omega)$  induces a deformation of *PZT*. Because the *PZT* is bonded to the structure, a force  $F(\omega)$  against that deformation is induced into the structure and the *PZT* as well. For 1-*dof* system, structural mechanical impedance of the host structure is obtained by the ratio of force  $F(\omega)$  to velocity  $\dot{u}(\omega)$  as follows (Liang *et al.* 1994)

$$Z_s(\omega) = \frac{F(\omega)}{\dot{u}(\omega)} = c + m \frac{\omega^2 - \omega_n^2}{\omega} \quad (1)$$

where  $c$  and  $m$  are the damping coefficient and the mass of the structure, respectively;  $\omega_n$  is the angular

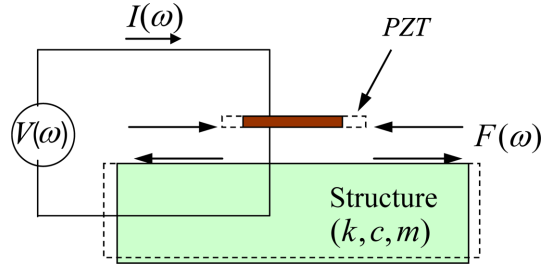


Fig. 3 Model of coupling interaction between PZT transducer and structure

natural frequency of the structure; and  $\omega$  is the angular frequency of the excitation voltage. As shown in Eq. (1), structural mechanical impedance is a function of mass, damping, and stiffness (i.e., stiffness is introduced from natural frequency,  $k = m\omega_n$ ). Thus, the change in structural parameters can be represented by the change in structural mechanical impedance.

In practice, the electric current  $I(\omega)$  is measured and then it is utilized to calculate electro-mechanical impedance as follows (Liang *et al.* 1994)

$$Z(\omega) = \frac{V}{I} = \left\{ i\omega \frac{w_a l_a}{t_a} \left[ \hat{\varepsilon}_{33}^T - \frac{1}{Z_a(\omega)/Z_s(\omega) + 1} d_{3x}^2 \hat{Y}_{xx}^E \right] \right\}^{-1} \quad (2)$$

where  $\hat{Y}_{xx}^E = (1 + i\eta)Y_{xx}^E$  is the complex Young's modulus of the PZT patch at zero electric field;  $\hat{\varepsilon}_{xx}^E = (1 - i\delta)\varepsilon_{xx}^E$  is the complex dielectric constant at zero stress;  $d_{3x}$  is the piezoelectric coupling constant in  $x$ -direction at zero stress;  $k = \omega\sqrt{\rho/\hat{Y}_{xx}^E}$  is the wave number where  $\rho$  is the mass density of the PZT patch; and  $w_a$ ,  $l_a$ , and  $t_a$  are the width, length, and thickness of the piezoelectric transducer, respectively. The parameters  $\eta$  and  $\delta$  are structural damping loss factor and dielectric loss factor of piezoelectric material, respectively.

As shown in Eq. (2), the electro-mechanical impedance,  $Z(\omega)$ , is a combining function of the mechanical impedance of the host structure,  $Z_s(\omega)$ , and that of the piezoelectric patch,  $Z_a(\omega)$ . Therefore, the change in structural parameters ( $k$ ,  $m$ ,  $c$ ) can be represented by the change in electro-mechanical impedance.

For damage monitoring using impedance-based method, the frequency range which should be utilized is an important issue. The frequency range should be selected appropriately in order to realize structural change in electro-mechanical impedance. Generally, if excitation frequency is not identical to natural frequency of structure (i.e.,  $\omega \neq \omega_n$ ), structural mechanical impedance takes the full term of Eq. (1). In this case, impedance of the structure is very large compared with mechanical impedance of the PZT (i.e.,  $Z_s(\omega) \gg Z_a(\omega)$ ). As a result, the term  $Z_a(\omega)/Z_s(\omega)$  is neglected and electro-mechanical impedance is approximated as

$$Z(\omega) \approx \left\{ i\omega \frac{w_a l_a}{t_a} \left[ \varepsilon_{33}^T - d_{3x}^2 \hat{Y}_{xx}^E \right] \right\}^{-1} \quad (3)$$

In Eq. (3), the contribution of structural mechanical impedance to electro-mechanical impedance is filtered out. Therefore, structural change may not be identified sensitively by electro-mechanical impedance. On the other hand, if PZT sensor is excited by a frequency matching with natural frequency

of the structure (i.e.,  $\omega = \omega_n$ ), structural mechanical impedance takes only the term of damping coefficient (i.e.,  $Z_s(\omega) = c$ ). Therefore, structural impedance for that frequency is comparable with mechanical impedance of the PZT, and electro-mechanical impedance is expressed as

$$Z(\omega) = \left\{ i\omega \frac{w_a l_a}{t_a} \left[ \varepsilon_{33}^T - \frac{1}{Z_a/c + 1} d_{3x}^2 \hat{Y}_{xx}^E \right] \right\}^{-1} \quad (4)$$

In Eq. (4), the contribution of structural mechanical impedance to electro-mechanical impedance is the damping coefficient  $c$ . This contribution causes resonant response in electro-mechanical impedance signature at the correspondent frequency. In other words, electro-mechanical impedance at resonance represents not only modal damping but also natural frequency of the structure. Therefore, structural change could be identified sensitively by the change in electro-mechanical impedance at resonant frequency.

### 2.1.3 Tendon-anchorage's impedance for prestress-loss monitoring

According to the analytical model of tendon-anchorage, an approach for prestress-loss monitoring is conducted by examining electro-mechanical impedance of the anchorage. Thus, a PZT should be bonded near by the contact region of anchorage. Considering the bearing plate is relatively more elastically-deformable than the anchor block (i.e., assuming the anchor block as rigid body), it is easier to capture the change in structural contact parameters if the PZT is attached on the bearing plate, as shown in Fig. 4. The main idea is that electro-mechanical impedance of the bearing plate is monitored to detect the change in structural parameters at the contact interface, since these parameters represent contact pressure (bearing stress) or prestress force.

In order to detect resonant range, the bearing plate and the PZT patch are simply modeled as 1-dof system by bearing plate's mass ( $m_b$ ), bearing plate's stiffness ( $k_b$ ) and equivalent contact stiffness ( $k_c$ ) as shown in Fig. 4. Then the equivalent structural stiffness ( $k_e^{\text{bearing}}$ ) can be computed as

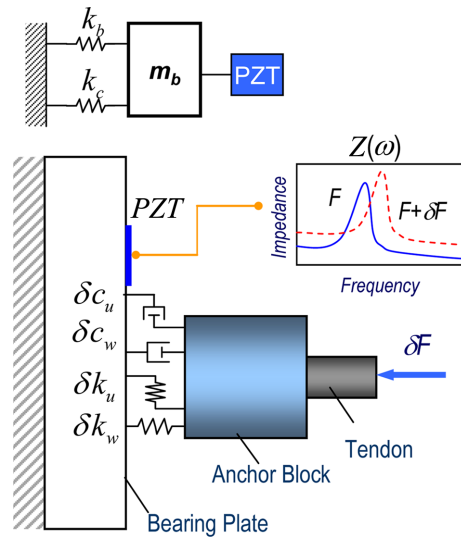


Fig. 4 Schematic of prestress-force monitoring by PZT sensor

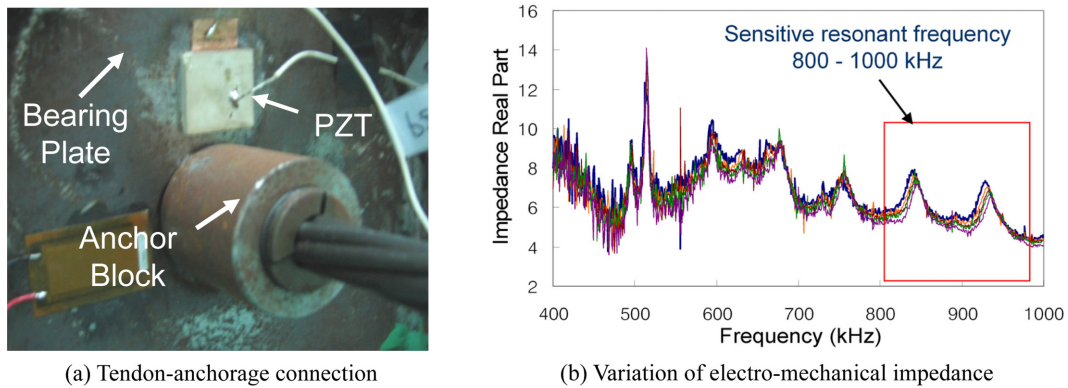


Fig. 5 Prestress-loss monitoring from anchorage impedance (Kim *et al.* 2010)

$$k_e^{\text{bearing}} = k_b + k_c \quad (5)$$

Suppose  $\beta = k_b/k_c$  is the ratio of bearing plate's stiffness to equivalent contact stiffness; then the equivalent structural stiffness is rewritten as follows

$$k_e^{\text{bearing}} = (1 + \beta)k_c \quad (6)$$

Assuming the bearing plate is clamped at one surface, its stiffness  $k_b$  would be very large. That leads to large value of the equivalent structural stiffness. Then, natural frequency of the system would be very high.

The verification experiment on a lab-scale tendon-anchorage was carried out by Kim *et al.* (2010). Fig. 5 illustrates the experimental setup and monitoring results obtained from that study. The variation of impedance due to prestress-loss was obviously obtained. However, impedance must be monitored in very high resonant frequency range like above 800 kHz. The experimental result proves that if the PZT is bonded at a very stiff region, the resonant response of the structure must be obtained at very high frequency excitation.

## 2.2 Smart PZT-interface for alternative prestress-loss monitoring

Although the conventional impedance-based method has shown the excellent performance to detect prestress-loss in tendon-anchorage, the method still has some limitations for applications. The drawbacks can be pointed out as follows:

(1) The effective frequency which indicates variation of prestress force could be very high, above 800 kHz (Kim *et al.* 2010). In this case, a high performance impedance analyzer is needed to capture such frequency range. Due to its weight, this device is not convenient to work out of laboratory. Moreover, the cost associated with the instrument system using this device is very high. Efforts to overcome these disadvantages have been carried out by adopting wireless impedance device (Mascarenas *et al.* 2007, Park *et al.* 2010). In order to apply the new approach, however, the measurable frequency range of 10 kHz-100 kHz of the wireless sensors should be dealt appropriately for impedance measurement as well as feature extraction.

(2) In order to employ the impedance-based method for prestress-loss detection, the frequency

range which is sensitive to prestress-loss has to be identified. Generally, the effective frequency range is varied dependent on target structures and usually determined by trial and error. This causes difficulty when applying the impedance-based method to real structure since the effective frequency range is almost unknown and may take much effort to obtain it by trial and error.

In order to overcome the above-mentioned limitations, an impedance-sensitive PZT-interface is designed as shown in Fig. 6. It is a thin plate equipped with a PZT patch. It is partly clamped at one end by a bearing plate and an anchor block, and freely vibrated at another end. The PZT sensor is bonded in the free part of the PZT-interface. Similarly, the contact interaction between two surfaces of the PZT-interface and the bearing plate and the anchor block can be modeled as interfacial structural parameters (i.e.,  $c_w, c_u, k_w, k_u$ ), as shown in Fig. 6(b). The main idea is that electro-mechanical impedance of the PZT-interface is monitored to detect the change in structural parameters at contact boundaries of the PZT-interface, since these parameters represents the change in interfacial bearing pressure or prestress force. Compared with the bearing plate and the anchor block which can be treated as rigid bodies, the PZT-interface is relatively more elastic and deformable.

In order to detect resonant range, the PZT-interface is simply modeled as 1-dof system by PZT-interface's mass ( $m_i$ ), PZT-interface's stiffness ( $k_i$ ) and equivalent contact stiffness ( $2k_c$ ) as shown in Fig. 6(b). The equivalent structural stiffness ( $k_e^{\text{interface}}$ ) is then modeled as 1-D serial system

$$k_e^{\text{interface}} = \frac{2k_c k_i}{2k_c + k_i} \tag{7}$$

Suppose  $\alpha = k_i/(2k_c)$  is the ratio of PZT-interface's stiffness to equivalent contact stiffness, the equivalent structural stiffness is rewritten as follows

$$k_e^{\text{interface}} = \left( \frac{\alpha}{1 + \alpha} \right) 2k_c \tag{8}$$

Substituting Eq. (8) into Eq. (6) leads to the ratio of equivalent stiffness parameter of the PZT-interface ( $k_e^{\text{interface}}$ ) to that of the bearing plate ( $k_e^{\text{bearing}}$ ) as follows

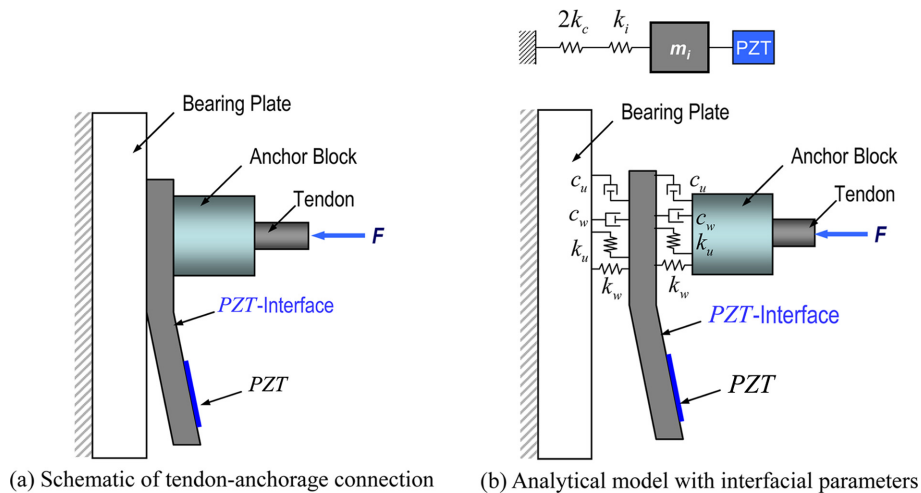


Fig. 6 Tendon-anchorage connection with PZT-interface

$$\frac{k_e^{\text{interface}}}{k_e^{\text{bearing}}} = \frac{2\alpha}{(1+\alpha)(1+\beta)} < \frac{2\alpha}{\beta} \quad (9)$$

From Eq. (9), the equivalent structural stiffness of *PZT*-interface system becomes much smaller than that of bearing plate system ( $k_e^{\text{interface}} \ll k_e^{\text{bearing}}$ ) if the *PZT*-interface's stiffness ( $k_i$ ) is much smaller than the bearing plate's stiffness ( $k_b$ ) (i.e.,  $\alpha \ll \beta$ ). Assume the mass of the *PZT*-interface ( $m_i$ ) is comparable with that of the bearing plate ( $m_b$ ), natural frequency of the *PZT*-interface system would be greatly reduced. In section 4, it will be experimentally proved that the resonant frequency of electro-mechanical impedance of *PZT*-interface is smaller than 50 kHz, which is measurable by wireless impedance sensor node.

### 3. Wireless impedance sensor node on *Imote2* platform

Recently, one of the important issues of *SHM* is to develop wireless smart sensor nodes for the efficient *SHM* system. The advantages of wireless sensor techniques over the conventional *SHM* system have been discussed by many researchers (Straser *et al.* 1998, Spencer *et al.* 2004, Kurata *et al.* 2005, Lynch and Loh 2006, Nagayama *et al.* 2007, Krishnamurthy *et al.* 2008, Ni *et al.* 2011). Generally, the cost associated with the wired *SHM* system can be greatly reduced by the adoption of wireless sensor nodes. Moreover, autonomous operations of the *SHM* are enabled by on-board computation embedded on the sensor nodes. For impedance-based *SHM*, wireless sensor node was first proposed by Mascarenas *et al.* (2007). Then, the sensor node has been modified by Park *et al.* (2010) and Taylor *et al.* (2010) by following the same concept.

In this study, we design a multiplexed impedance sensor board, so called *SSeL-I16*, which is working on the high performance *Imote2* sensor platform. The main board of the *Imote2* incorporates a low-power, high-speed *X*-scale process, *PXA27x*, and a wireless radio, *CC2420*. The amount of memory for programming and data repository is also very large. The *Imote2* has 256 kB of integrated *SRAM*, 32 MB of external *SDRAM*, and 32 MB of program flash memory. The combined *Imote2/SSeL-I16* sensor node has the capability to measure electro-mechanical impedances from multiple *PZT* patches. The design schematic of the *Imote2/SSeL-I16* sensor node is given in Fig. 7.

The components of the impedance sensor board *SSeL-I16* and the *Imote2* platform are pointed out in Fig. 8. The main component of the sensor node is the *AD5933* impedance chip. The *AD5933* was firstly used in the wireless impedance device developed by Mascarenas *et al.* (2007). This impedance chip has the capability of measuring electric impedance up to 100 kHz. The *AD5933* impedance

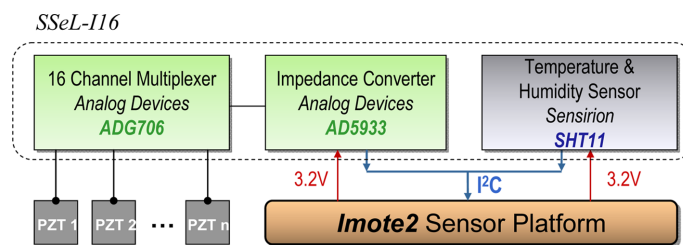


Fig. 7 Design of impedance sensor node

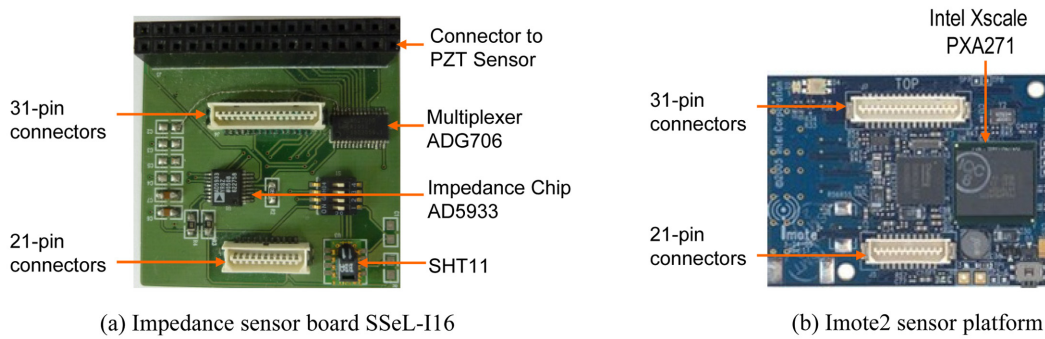


Fig. 8 Components of SSeL-I16 and *Imote2* platform

chip has the following embedded multi-functional circuits: function generator, digital-to-analog (*D/A*) converter, current-to-voltage amplifier, anti-aliasing filter, *A/D* converter, and discrete Fourier transform (*DFT*) analyzer. The *AD5933* outputs real and imaginary values of impedance for a target frequency of interest and transmits the values into a microcontroller. In this design, an *ADG706* multiplexer is integrated into *SSeL-I16* board to allow monitoring impedance from up to sixteen *PZT* sensors by a single sensor node. The 16 channel multiplexer is very useful to build an efficient monitoring system in real prestressed structures where many *PZT* sensors should be attached to cover the whole prestressed zone. A *SHT11* sensor is also integrated into *SSeL-I16* board to monitor environmental temperature and humidity. The *SSeL-I16* board connects to *Imote2* through 31-pin and 21-pin connectors in one side. It also allows other external devices to connect to *Imote2* by returning the connectors in another side.

For operation, embedded software of the *Imote2/SSeL-I16* is programmed on TinyOS platform. The wireless monitoring system is illustrated in Fig. 9. The system starts when the user makes a

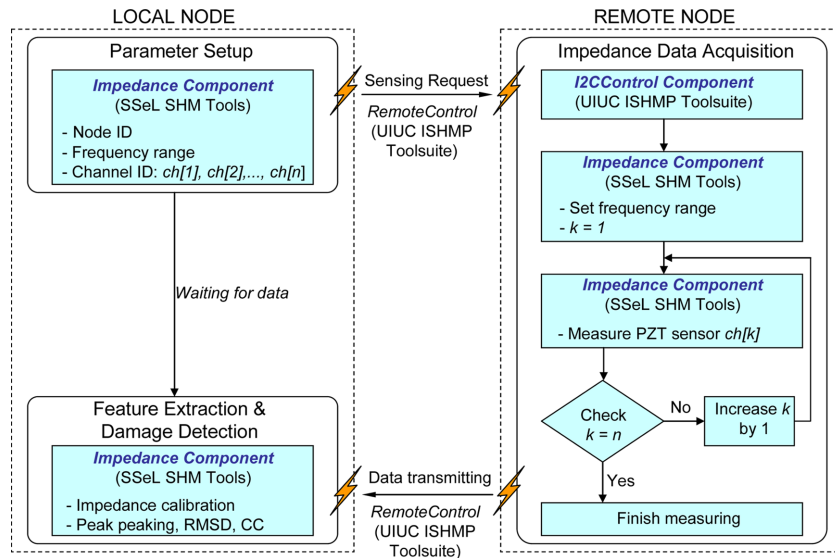


Fig. 9 Embedded software of *Imote2/SSeL-I16*

measuring request to remote node from local node. Frequency range, sweeping interval and sensor channels are transmitted to local node through “*RemoteControl*” component. After receiving request, the remote node measures both real and imaginary parts of impedance from the defined channels, sequentially. When impedance signatures of all defined channels are completely measured, data are transmitted to the local node. At the local node, the raw impedance signatures are calibrated and processed to feature extraction and damage monitoring using resonant frequency, root mean square deviation (*RMSD*) or cross correlation (*CC*) of impedance signatures. It is worth noting that, the “*RemoteControl*” component for wireless transmitting and the “*I2CControl*” component for *TWI* protocol controlling are provided from *ISHMP Services Toolsuite* (Illinois Structural Health Monitoring Project 2010); and the “*Impedance*” component is newly developed in *SSEL-SHM Tools* by our research group.

#### 4. Experimental verification of prestress-loss monitoring by impedance sensor node and *PZT*-interface

##### 4.1 Experimental setup

A lab-scale tendon-anchorage connection as shown in Fig. 10 was utilized to investigate the variation of impedance signature with the loss of prestress force. A *PZT*-interface was installed to the tendon-anchorage connection as the way schematized in Fig. 6. Impedance signature of the *PZT*-interface was measured by an impedance sensor node *Imote2/SSEL-I16* placed near the anchorage system. The sensor node was powered by three *D*-Cell batteries which ensure the power supply for the sensor node during the test. A base station which included an *Imote2* associated with an interfacial board *IIB2400* and a computer was placed at 5 m distant from the tendon-anchorage connection. The *IIB2400* provides two ports from *Imote2* to the computer, one for sending command and receiving debug messages from remote node, and one for transferring measured data. A command-line interface, *Cygwin* software (Red Hat 2012), was utilized to operate the wireless system. For comparison purpose, impedance of the *PZT*-interface was also measured by a commercial impedance analyzer *HIOKI 3532-50*.

As summarized in the first two columns of Table 1, five prestress levels between 54.9 kN and 98 kN were applied to the tendon-anchorage connection. The first level *C0* (i.e., prestress force of 98 kN) was considered as designed force. The others represented various prestress-loss levels due to uncertainty conditions. The first damage case, *C1*, was simulated by reducing 16% of designed force. Subsequently, for other damage cases, additional gradual losses of about 10% were sequentially released off the tendon. Among them, the maximum loss 44% can be considered as severe reduction of prestress force.

##### 4.2 Prestress-loss versus impedance variation

###### 4.2.1 Frequency range selection

According to the datasheet of the *AD5933*, the recommend measurable impedance is larger than 1 k $\Omega$ . The accuracy decreases when measuring impedance smaller than 1 k $\Omega$  of magnitude. For the *PZT*-interface, measurement by the sensor node becomes inaccurate at frequency range over 50 kHz where magnitude of impedance becomes very small (i.e., below 200 $\Omega$ ). Therefore, impedance of the

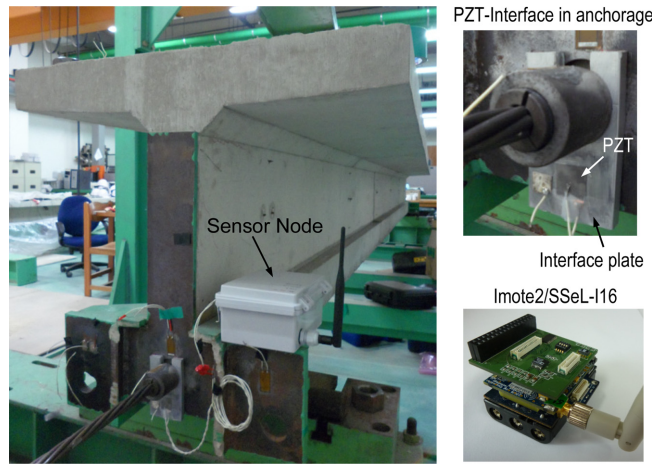


Fig. 10 Experiment setup on tendon-anchorage connection

Table 1 Impedance analysis for five prestress forces by wireless system

Case	Inflicted prestress force		Resonant freq. (kHz)	Change in impedance		Predicted $\Delta P/P_0$ (%)	
	$P$ (kN)	$\Delta P/P_0$ (%)		Freq. Shift (kHz)	CCD (%)	by Eq. (11) (Freq. Shift)	by Eq. (12) (CCD)
$C_0$	98	0	24.42	0	0.2	0 (0)	0.3 (0.3)
$C_1$	82.3	16.0	24.24	-0.18	13.2	13.6 (2.4)	8.7 (7.3)
$C_2$	73.5	25.0	24.22	-0.2	21.2	15.2 (9.8)	17.6 (7.4)
$C_3$	64.7	34.0	23.96	-0.46	38.3	34.8 (0.8)	34.9 (0.9)
$C_4$	54.9	44.0	23.76	-0.66	47.8	50.0 (6.0)	50.2 (6.2)

\*Parentheses indicate differences (%) of predicted prestress-loss with respect to inflicted prestress-loss

*PZT*-interface in the range 10 kHz-50 kHz is examined for its capability of prestress-loss detection. Fig. 11 shows impedance signatures of the *PZT*-interface in the frequency range 10 kHz-50 kHz with 501 points by the *Imote2/SSeL-I16* and the impedance analyzer at prestress level  $C_0$ . As shown in Fig. 11, both real part and imaginary part of impedance measured by the sensor node are well matched with those by the commercial system. It is worth noting that the *HIOKI 3532-50* is very costly (US\$ 10,000) compared with the *Imote2/SSeL-I16* (US\$ 350).

Generally, real part of electro-mechanical impedance contains much more information of structural behaviors than imaginary part (Sun *et al.* 1995, Park *et al.* 2003). Therefore, real part of impedance is examined for prestress-loss monitoring. Fig. 12 shows impedance signatures of the *PZT*-interface for the healthy state  $C_0$  and four prestress-loss cases  $C_1$ - $C_4$ . In the wide frequency band from 10 kHz to 50 kHz (Fig. 12(a)), it is found that the impedance signatures in non-resonant regions (i.e., 10 kHz-20 kHz and 30 kHz - 50 kHz) are little changed due to prestress-loss. That is because impedance signatures in these ranges are associated with only *PZT* properties as clarified in Eq. (3). On the other hand, the impedance signature in resonant range 20 kHz-30 kHz is significantly varied when tendon force decreases. This implies the contribution of structural impedance to electro-mechanical impedance is considerable in resonant range, which is explained in Eq. (4). Thus, the impedance signatures in the range 20 kHz - 30 kHz should be examined for

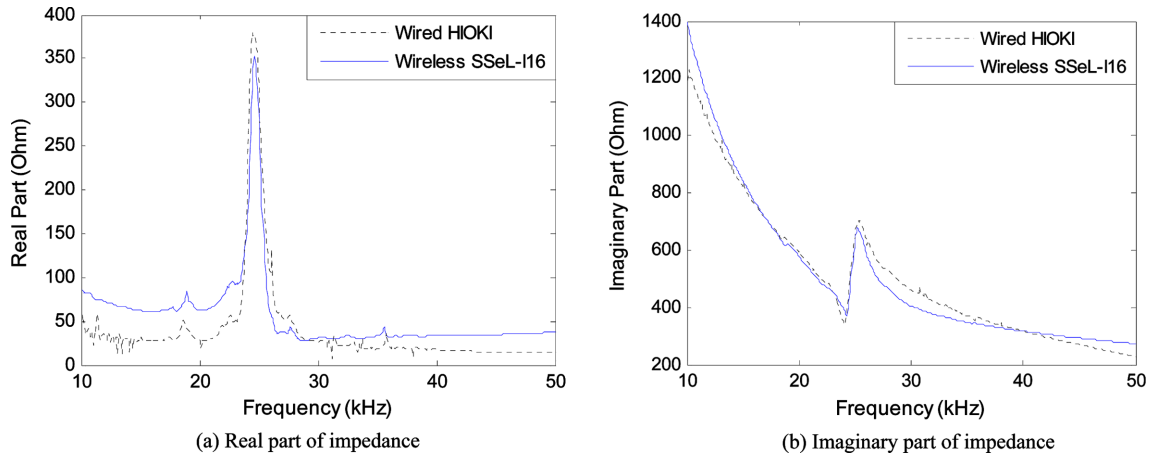


Fig. 11 Impedance of *PZT*-interface by wired and wireless system under prestress force *C0*

prestress-loss detection.

#### 4.2.2 Monitoring of prestress-loss

Electro-mechanical impedance technique is very sensitive to changes in near field boundary condition. In this case, the *PZT*-interface is an additional item sandwiched between the bearing plate and the anchor block. Slight changes in the position or configuration of their interfaces may vary the impedance signatures significantly, affecting the accuracy of electro-mechanical impedance signatures. Considering the fact, the relative change of impedances before and after prestress-loss occurrence, in which the difference in baseline measurement is canceled out, is quantified by frequency shift and cross correlation deviation (*CCD*).

As shown in Fig. 12(b), impedance signatures in the range 20 kHz - 30 kHz tend to shift left with the loss of prestress force. This implies that modal stiffness of the *PZT*-interface is decreased with the reduction of prestress force. The detailed peak frequencies and frequency-shifts for the four damaged cases are outlined in Table 1. Also, the frequency-shifts calculated by the *Imote2/SSeL-116*

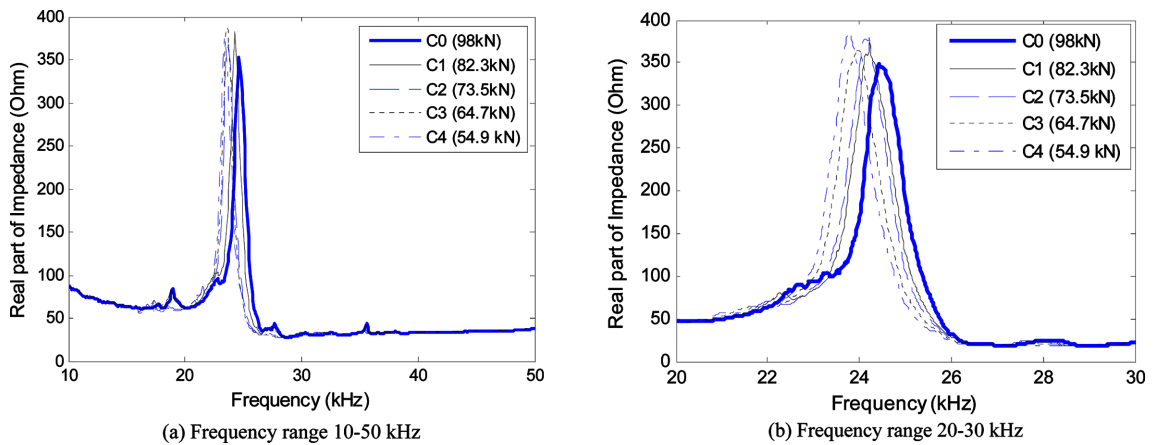


Fig. 12 Impedance signatures of *PZT*-interface under various prestress forces

and by the commercial wired system under various prestress forces are graphically shown in Fig. 13(a). The results by the wireless system show good agreement with those by the commercial system. It is observed that the frequency-shift varies almost linearly with the prestress-loss. Also, the fluctuation of frequency-shift is expectedly found as small as 0.02 kHz which is correspondent to the resolution of impedance signature. It is worth noting that the variation of resonance impedances which represents the change in modal damping of the PZT-interface can be observed. However, the pattern of this variation is not very clear to be considered as a damage indicator.

Since prestress-loss mainly causes the horizontal shift of impedance, CCD index is utilized to quantify the change of the whole impedance signatures. The CCD index is calculated as follows:

$$CCD = 1 - \frac{1}{\sigma_Z \sigma_{Z^*}} E \{ [Re(Z_i) - Re(\bar{Z})][Re(Z_i^*) - Re(\bar{Z}^*)] \} \quad (10)$$

where  $E[\cdot]$  is the expectation operation;  $Re(Z_i)$  signifies the real parts of the electro-mechanical impedances of the  $i^{th}$  frequency before and after damage;  $Re(\bar{Z})$  signifies the mean values of impedance signatures (real part) before and after damage; and  $\sigma_Z$  signifies the standard deviation values of impedance signatures before and after damage. Note that the asterisk (\*) denotes the damaged state.

Generally, CCD is sensitive to horizontal shift, but less sensitive to vertical shift of impedance signature. Therefore, the changes in PZT's properties, which usually cause vertical shift of impedance signature, little affect to the CCD. The CCD indices computed by Eq. (10) for the four damaged cases are listed in Table 1. Fig. 13(b) shows the CCD index calculated by the wired and wireless systems according to the increment of prestress-loss. The results by the two systems are very close to each other. It is obvious that the CCD index increases almost linearly with the reduction of prestress force. It is worth noting that the variation of CCD is found within 1.6% for a particular prestress-loss case. This fluctuation may affect the accuracy of monitoring results for small amount of prestress-loss (e.g., case C1), but little affects the detection accuracy for severe prestress-loss (e.g., case C4).

### 4.3 Prestress-loss prediction

Fig. 13 shows the relationships between prestress-loss and frequency-shift and CCD of impedance signatures, respectively, which are also listed in Table 1. From these analyses, the following empirical formulas are obtained to predict the prestress-loss

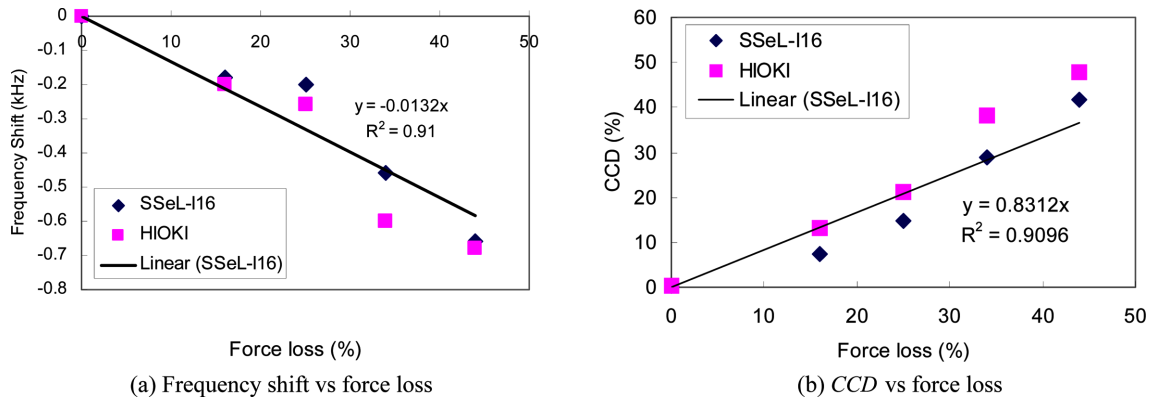


Fig. 13 Frequency shift and CCD of impedance signatures due to prestress-loss

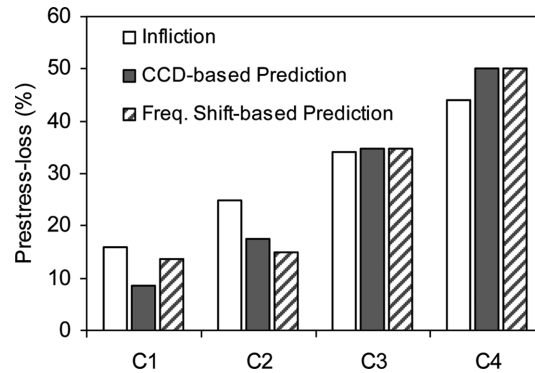


Fig. 14 Prestress-loss prediction based on impedance variation

$$\frac{\Delta P}{P_0}(\%) = -\frac{\Delta f}{0.0132} \quad (11)$$

and

$$\frac{\Delta P}{P_0}(\%) = \frac{CCD(\%)}{0.8312} \quad (12)$$

where  $\Delta P$  is the amount of prestress reduction,  $P_0$  is the designed prestress force (i.e.,  $C0$ ), and  $\Delta f$  is the frequency shift (kHz) with regarding to resonant frequency at the designed prestress force; and the term  $\Delta P/P_0$  denotes the relative loss of prestress force.

Using Eqs. (11) and (12), predicted prestress-losses are computed as shown in Table 1 and Fig. 14. It is shown that prediction results using frequency-shift are very similar with those using the *CCD* index. This implies the *CCD* index is highly associated with the horizontal shift of impedance. Compared with the infliction, the prediction results show relatively good agreement. Except the large error of the prediction based on frequency shift in case *C2* (i.e., 9.8%), other prestress-loss cases were well predicted with small errors (i.e., 0.8%~7.4%). From the prediction results, frequency shift and *CDD* of impedance are found to be the good indicators to detect prestress-loss in tendon-anchorage connection.

## 5. Conclusions

In this study, a smart *PZT*-interface for wireless impedance-based prestress-loss monitoring in tendon-anchorage connection was introduced. The *PZT*-interface was designed in order to realize sensitively the change in electro-mechanical impedance due to prestress-loss. The relationship between prestress force and structural parameters of the anchorage contact interface was described by an analytical model. Based on the model, an impedance-based method for prestress-loss monitoring was established using the impedance-sensitive *PZT*-interface. Also, the design of wireless impedance sensor node which is interacted with the *PZT*-interface was outlined. The performance of the smart *PZT*-interface along with the wireless impedance sensor node was evaluated on a lab-scale tendon-anchorage of prestressed concrete girder. The change in impedance due to prestress-loss was estimated by frequency shift and *CCD* of the impedance signature.

From the experimental verification, the implementation of the smart PZT-interface was successful in indicating various prestress-losses in the tendon-anchorage connection. Electro-mechanical impedance of the PZT-interface was sensitive to prestress-loss even the examined frequency range was rather low, smaller than 50 kHz. Frequency shift and CDD index were the good indicators to realize the change in impedance of PZT-interface due to prestress-loss. For wireless application, the impedance sensor node designed in this study showed the good performance on impedance-based monitoring of prestress-loss. The use of this device is very promising since it is portable, inexpensive and enable for wireless operation. However, the sensor node needs to be improved to monitor impedance of low amplitude (i.e., below 200  $\Omega$ ).

Although the good results were achieved, further studies must be carried out. Firstly, this study is based solely on the experiment with single tendon, which needs to be verified in a more practical model with multiple tendons. Secondly, research efforts are needed to examine effects of environmental factors such as temperature and humidity on monitoring results.

## Acknowledgements

This work was supported by the Innovations in Nuclear Power Technology of the Korean Institute of Energy Technology Evaluation and Planning (KETEP) grant funded by the Korean Government Ministry of Knowledge Economy (KETEP-2010620100210). The graduate student involved in this research was also partially supported by the Brain Korea 21 (BK21) program of Korean Government.

## References

- Bhalla, S. and Soh, C.K. (2003), "Structural impedance based damage diagnosis by piezo-transducers", *Earthq. Eng. Struct. D.*, **32**(12), 1897-1916.
- Red Hat (2012), Available from <<http://cygwin.com>>.
- Fasel, T.R., Sohn, H., Park, G. and Farrar, C.R. (2005), "Active sensing using impedance-based arx models and extreme value statistics for damage detection", *Earthq. Eng. Struct. D.*, **34**(7), 763-785.
- Illinois Structural Health Monitoring Project (2010), Available from <http://shm.cs.uiuc.edu>.
- Johnson, K.L. (1985), *Contact mechanics*, Cambridge University Press, Cambridge.
- Kim, B.H. and Park, T. (2007), "Estimation of cable tension force using the frequency-based system identification method", *J. Sound Vib.*, **304**(3-5), 660-676.
- Kim, J.T., Park, J.H., Hong, D.S., Cho, H.M., Na, W.B. and Yi, J.H. (2009), "Vibration and impedance monitoring for prestress-loss prediction in PSC girder bridges", *Smart Struct.Syst.*, **5**(1), 81-94.
- Kim, J.T., Park, J.H., Hong, D.S. and Park, W.S. (2010), "Hybrid health monitoring of prestressed concrete girder bridges by sequential vibration-impedance approaches", *Eng. Struct.*, **32**(1), 115-128.
- Kim, J.T., Na, W.B., Park, J.H. and Hong, D.S. (2006), "Hybrid health monitoring of structural joints using modal parameters and EMI signatures", *Proceeding of the SPIE*, San Diego, USA.
- Krishnamurthy, V., Fowler, K. and Sazonov, E. (2008), "The effect of time synchronization of wireless sensors on the modal analysis of structures", *Smart Mater. Struct.*, **17**(5), 1-13.
- Kurata, N., Spencer, B.F. and Ruiz-Sandoval, M. (2005), "Risk monitoring of buildings with wireless sensor networks", *Struct. Health Monit.*, **12**(3-4), 315-327.
- Li, H., Ou, J.P. and Zhou, Z. (2009), "Applications of optical fiber Bragg gratings sensing technology-based smart stay cables", *Opt. Laser Eng.*, **47**(10), 1077-1084.
- Liang, C., Sun, F.P. and Rogers, C.A. (1994), "Coupled electro-mechanical analysis of adaptive material - Determination of the actuator power consumption and system energy transfer", *J. Intell. Mat. Syst.Str.*, **5**(1),

12-20.

- Lynch, J.P. and Loh, K. (2006), "A summary review of wireless sensors and sensor networks for structural health monitoring", *Shock Vib.*, **38**(2), 91-128.
- Mascarenas, D.L. (2006), *Development of an impedance-based wireless sensor node for monitoring of bolted joint preload*, MS Thesis, Department of Structural Engineering, University of California, San Diego, USA.
- Mascarenas, D.L., Todd, M.D., Park, G. and Farrar, C.R. (2007), "Development of an impedance-based wireless sensor node for structural health monitoring", *Smart Mater. Struct.*, **16**(6), 2137-2145.
- Nagayama, T., Sim, S.H., Miyamori, Y. and Spencer, B.F. (2007), "Issues in structural health monitoring employing smart sensors", *Smart Struct. Syst.*, **3**(3), 299-320.
- Ni, Y.Q., Li, B., Lam, K.H., Zhu, D.P., Wang, Y., Lynch, J.P. and Law, K.H. (2011), "In-construction vibration monitoring of a super-tall structure using a long-range wireless sensing system", *Smart Struct. Syst.*, **7**(2), 83-102.
- Park, G., Sohn, H., Farrar, C. and Inman, D. (2003), "Overview of piezoelectric impedance-based health monitoring and path forward", *Shock Vib.*, **35**(6), 451-463.
- Park, J.H., Kim, J.T., Hong, D.S., Mascarenas, D. and Lynch, J.P. (2010), "Autonomous smart sensor nodes for global and local damage detection of prestressed concrete bridges based on accelerations and impedance measurements", *Smart Struct. Syst.*, **6**(5), 711-730.
- Park, G., Cudney, H.H. and Inman, D.J. (2001), "Feasibility of using impedance-based damage assessment for pipeline structures", *Earthq. Eng. Struct. D.*, **30**(10), 1463-1474.
- Ritdumrongkul, S., Abe, M., Fujino, Y. and Miyashita, T. (2004), "Quantitative health monitoring of bolted joints using a piezoceramic actuator-sensor", *Smart Mater. Struct.*, **13**(1), 20-29.
- Sohn, H., Farrar, C.R., Hemez, F.M., Shunk, D.D., Stinemates, D.W. and Nadler, B.R. (2003), *A review of structural health monitoring literature: 1996-2001*, Los Alamos National Laboratory Report, LA-13976-MS, Los Alamos, NM.
- Spencer, B.F., Ruiz-Sandoval, M.E. and Kurata, N. (2004), "Smart sensing technology: opportunities and challenges", *Struct. Health Monit.*, **11**(4), 349-368.
- Straser, E.G. and Kiremidjian, A.S. (1998), *A modular, wireless damage monitoring system for structure*, Technical Report 128, John A. Blume Earthquake Engineering Center, Stanford University, Stanford, CA.
- Sun, F.P., Chaudhry Z., Liang, C. and Rogers C.A. (1995), "Truss structure integrity identification using PZT sensor-actuator", *J. Intell. Mat. Syst. Str.*, **6**(1), 134-139.
- Taylor, S.G., Farinholt, K.M., Park, G., Todd M.D. and Farrar, C.R. (2010), "Multi-scale wireless sensor node for health monitoring of civil infrastructure and mechanical systems", *Smart Struct. Syst.*, **6**(5-6), 661-673.
- Yang, Y., Hu, Y. and Lu, Y. (2008), "Sensitivity of PZT impedance sensors for damage detection of concrete structures", *Sensors*, **8**(1), 327-346.
- Yun, C.B and Min, J. (2010), "Smart sensing, monitoring, and damage detection for civil infrastructures", *KSCE J. Civil Eng.*, **15**(1), 1-14.
- Zagrai, A.N. and Giurgiutiu, V. (2001), "Electro-mechanical impedance method for crack detection in thin plates", *J. Intell. Mater. Syst. Str.*, **12**, 709-718.
- Zui, H., Shinke, T. and Namita, Y. (1996), Practical formulas for estimation of cable tension by vibration method, *J. Struct. Eng. - ASCE*, **122**, 651-656.